Journal of the European Ceramic Society xxx (xxxx) xxx

Contents lists available at ScienceDirect

Journal of the European Ceramic Society

journal homepage: www.elsevier.com/locate/jeurceramsoc

Low cost structured photocatalysts from stereolithography of colorless pharmaceutical glass

Akansha Mehta [a,*], Paulina Ozog [a], Arish Dasan [a], Jozef Kraxner [a], Hamada Elsayed [c], Luca Grigolato [c], Dusan Galusek [a,b], Enrico Bernardo [c]

[a] FunGlass—Centre for Functional and Surface Functionalized Glass, Alexander Dubček University of Trenčín, 91150 Trenčín, Slovakia
[b] Joint Glass Centre of the IIC SAS, TnUAD and FChFT STU, 91150 Trenčín, Slovakia
[c] Department of Industrial Engineering, Università degli Studi di Padova, 35131 Padova, Italy

ARTICLE INFO

Keywords:
Upcycling
3D scaffolds
TiO_2
Photocatalysis
Degradation of dyes

ABSTRACT

The present study is dedicated to the manufacturing of highly porous triply periodic minimal surface (TPMS) constructs, fabricated from recycled end of life borosilicate pharmaceutical glass employing masked stereolithography. The structures were prepared from a simple blend of photocurable resin with glass powder (<38 μm). The gyroid model was selected with the porosity varying from 75 to 90%. Hot stage microscopy was applied to examine the glass sintering behaviour to improve the translucency of the 3D scaffolds. The obtained 3D scaffolds were dip-coated with TiO_2 and further utilized for the photocatalytic degradation of dyes. The photocatalytic efficiency of the 3D scaffolds was evaluated by the degradation of methylene blue in water. It was found that 3D scaffolds coated with TiO_2 showed a 40% higher degradation rate in comparison to bare 3D scaffolds under UV irradiation, which determines the significant role of TiO_2 in the organic dye degradation. The better efficiency of 3D scaffolds coated with TiO_2, compared with uncoated BSG 3D scaffolds is attributed to a better recombination rate, and the migration of electrons to the surface of the scaffold, where the charges participate in the photodecomposition of MB dye. The efficiency of the scaffolds was assessed for five consecutive cycles. The degradation efficiency after the fifth cycle was 75%, confirming the stability of the system.

1. Introduction

Glass is a resource and recycling glass to replace virgin raw materials is beneficial for the environment, the climate, and the economy [1]. Glass waste can be classified into two main categories: Glass cullet, which after collection have been sourced and it is suitable for reuse, and glass fines which are considered unsuitable for recycling [2,3]. This fine glass cannot be reused to produce container glass due to chemical incompatibility and a different melting temperature [4]. In some countries, unrecycled glass is landfilled or stockpiled. This attitude represents not only a significant waste of resources but also pollutes the earth and environment [5,6].

A sustainable alternative is upcycling which stands for a combination of 'upgrading' (adding value) and 'recycling' (reusing). Manufacturing of functional materials from glass waste with the use of a suitable and effective technical approach thus acquired increasing attention [7]. Recent emerging manufacturing processes such as 3D printing represents a beneficial tool for the development of a circular economy model. Additive manufacturing (AM) allows waste to be recovered and products to be recycled, thereby extending their life. Several research studies have been directed towards the development of additively manufactured ceramic components from waste materials [8–10].

The extrusion-based AM techniques facilitate the fabrication of 3D scaffolds with interconnected porous network by extruding and depositing ceramic slurry through fine nozzles, according to predetermined printing paths. However, the conventional extrusion-type AM technique is restricted in terms of adequate design outputs and nozzle size [10-12]. Instead, photopolymerization- AM techniques like stereolithography (SL) offer the desired quality, tunable porosity, and the possibility of fabricating complex void structures via computer-aided design (CAD) [13]. In SL, the objects are fabricated using photopolymer resin, that can polymerize and form a rigid body. Despite various advantages, there are also several limitations of the method. High viscosity of the ink reduces the printing precision, which causes the sedimentation of glass powder in the liquid resin, increases the complexity of recoating the uniform layers, and the scattering of particles in the suspension results in

* Corresponding author.
E-mail address: akansha.akansha@tnuni.sk (A. Mehta).

https://doi.org/10.1016/j.jeurceramsoc.2023.12.080
Received 2 August 2023; Received in revised form 19 December 2023; Accepted 22 December 2023
Available online 23 December 2023

Table 1
Conditions of heat treatment (700 °C (TT1), 750 °C (TT2) and 780 °C (TT3)) of BSG 3D scaffolds.

Thermal treatment 1 (TT1)	Thermal treatment 2 (TT2)	Thermal treatment 3 (TT3)
1°C·min^{-1}, 120°C, 0 h	1°C·min^{-1}, 120°C, 0 h	1°C·min^{-1}, 120°C, 0
0.5°C·min^{-1}, 330°C, 10 h	0.5°C·min^{-1}, 350°C, 12 h	0.2°C·min^{-1}, 370°C, 12 h
0.5°C·min^{-1}, 510°C, 6 h	0.5°C·min^{-1}, 520°C, 6 h	0.5°C·min^{-1}, 570°C, 6 h
10°C·min^{-1}, 700°C, 1 h	10°C·min^{-1}, 750°C, 1.5 h	10°C·min^{-1}, 780°C, 1.5 h
Free cooling	Free cooling	Free cooling

reduction of the printing resolution. [14,15]. The sedimentation of glass powders is highly dependent on the particle size of the powders. Aggregation usually occurs for the smaller particles; this can be prevented by the addition of surfactants. Considering the issues mentioned above, the present study is focused on the effect of solid loading and the addition of surfactants, and its influence on the quality and performance of AM structures with different porosities. [16,17].

Recently, the interest in associating AM with water treatment has increased considerably, especially in the fabrication of ceramic membranes for water treatment applications [18]. The need to treat the contaminated water before its release into the environment is an inevitable challenge. The most common sources of contaminated water are oil and gas refineries, petrochemical, pharmaceutical, metallurgical, dye, and food industries [19,20]. The extensive use of synthetic dyes in numerous industries harms the environment and seriously affects humans causing health issues such as quadriplegia, increased heart rate, vomiting, tissue necrosis, and cyanosis [21].

Photocatalysis arises as a promising technology for degradation of organic pollutants and dyes for water treatment applications. Titanium dioxide (TiO_2) is the most frequently used semiconductor catalyst for the photocatalytic processes owing to its unique properties such as high chemical stability, low toxicity, relative availability at low cost, and high oxidation rate of organic pollutants [22,23]. Different techniques are used for coating TiO_2 on the top surface of ceramic membranes. One of the most promising methods is dip-coating. It is applied to create a crack-free and uniform layer of TiO_2 on ceramic membranes that helps the light efficiently scatter over the entire scaffold, It also helps maintain the translucency of the scaffolds, which ultimately leads to higher photocatalytic activity [24,25].

In this perspective, the current study aims at the optimization of an AM process, utilizing boro-aluminosilicate (BSG) waste glasses to create durable, self-supporting 3D photocatalytic TiO_2 scaffolds (3D BSG-TiO_2) applied as membranes for the degradation of organic dyes. The fabrication of 3D BSG-TiO_2 scaffolds involves several optimization steps like geometry, porosity, solid loading, and then viscous flow sintering at suitable temperatures to achieve translucency even after TiO_2 coating to achieve maximum photocatalytic efficiency.

2. Materials, instrumentation and methods

Pharmaceutical boro-aluminosilicate glass (referred to as 'BSG', provided by Stevanato Group, chemical composition: SiO_2 = 72 wt%, Al_2O_3 = 7 wt%, B_2O_3 = 12 wt%, Na_2O = 6 wt%, K_2O= 2 wt%, CaO = 1

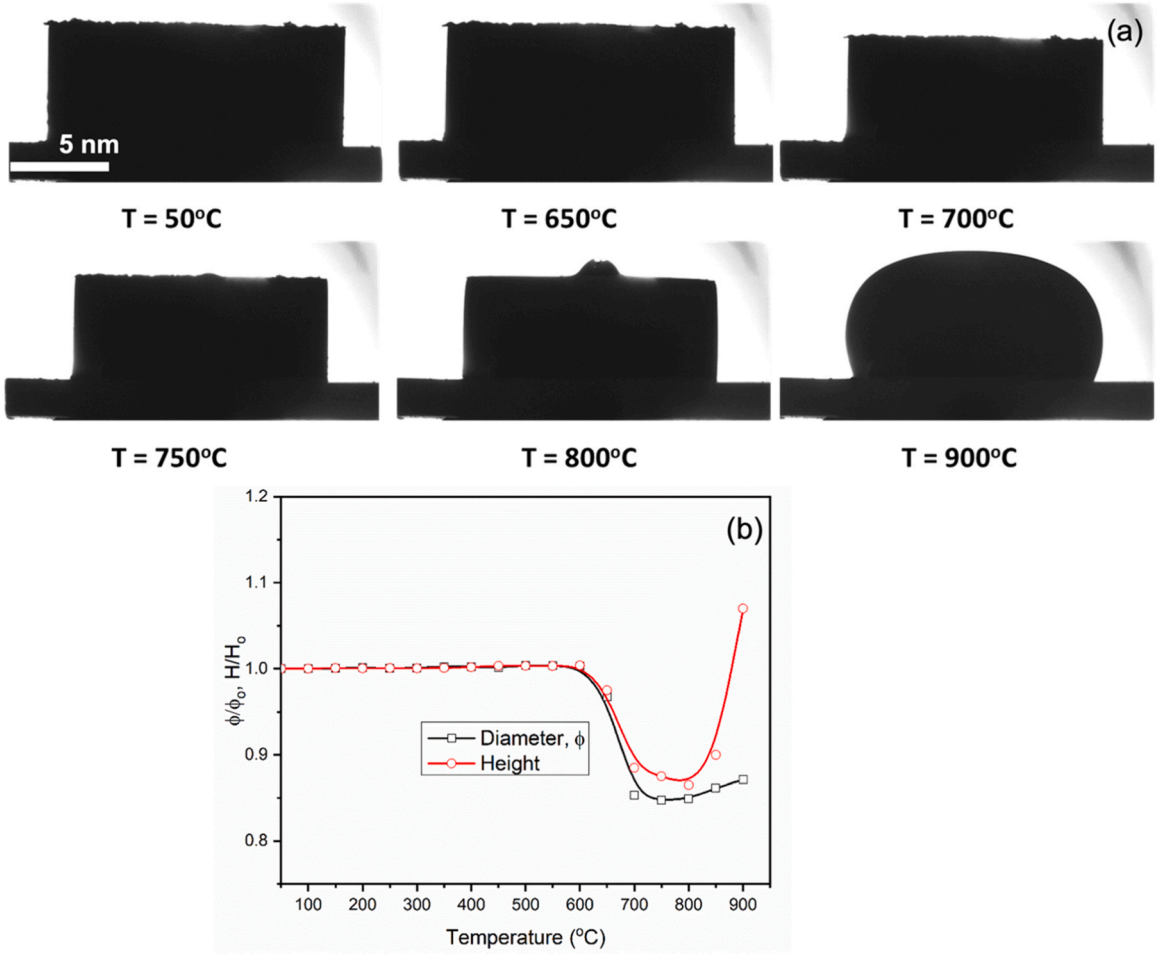

Fig. 1. HSM study of a BSG glass powder compact: (a) changes in morphology; optimized sintering temperature observed between 700 °C and 800 °C (b) changes in relative diameter and relative height of the pellet.

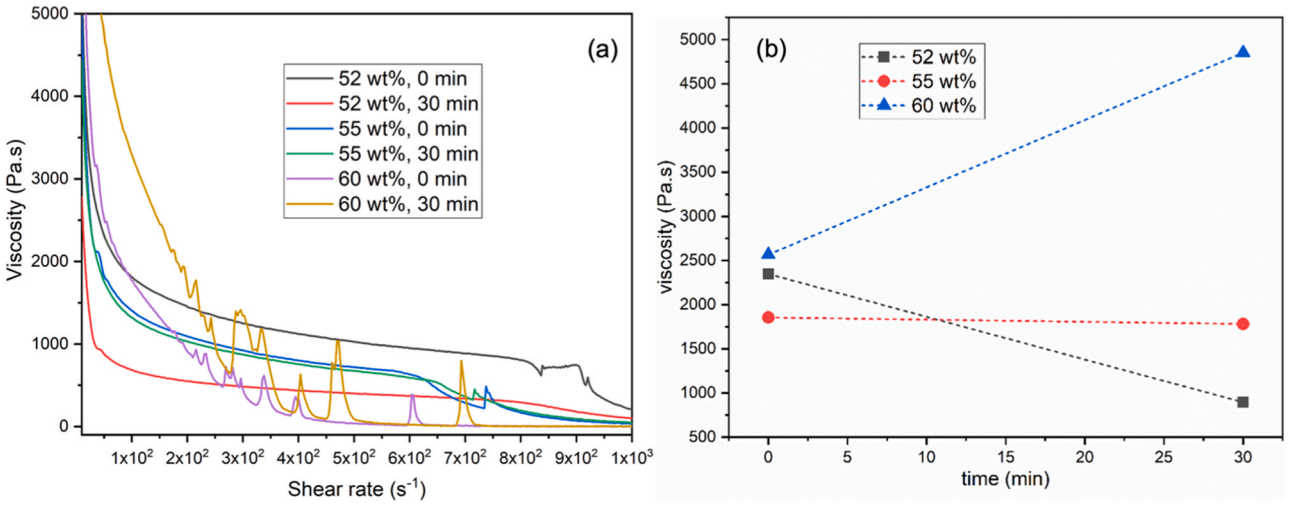

Fig. 2. (a) Viscosity of BSG suspensions with different solid loading (52 wt%, 55 wt% and 60 wt%) as a function of shear rate and time; (b) viscosity of BSG suspensions with different solid loading as a function time at the shear rate of 50 s^{-1}, no significant viscosity changes after 30 min setting time.

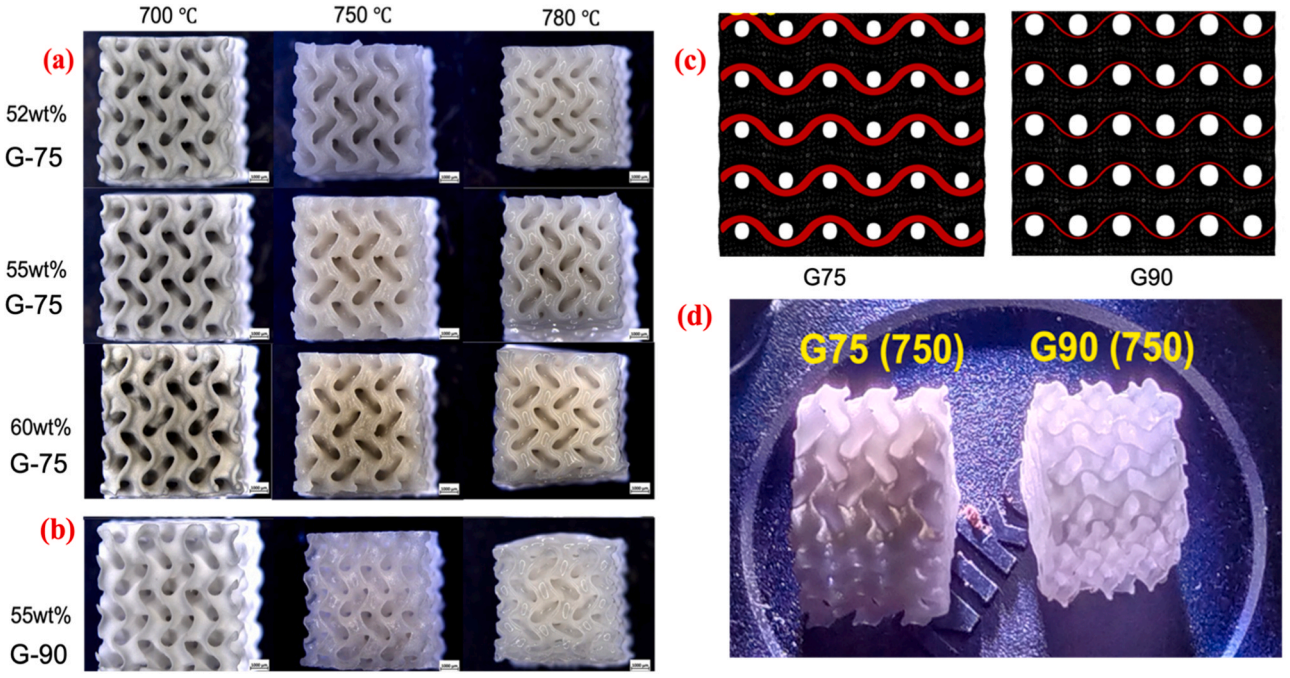

Fig. 3. (a) Stereomicroscope images of the BSG gyroid scaffolds prepared from slurries with different solid loadings and sintered at various temperatures (b) BSG gyroid scaffolds with a higher porosity G-90 after sintering at different temperatures (c) Reference three-dimensional gyroid models adopted for MSLA scaffolds (d) Comparison of translucency with G-75 and G-90 using LED light.

wt%, BaO < 0.1 wt%) was used as the starting material. Glass vials were crushed, ball milled and sieved under 40 μm. The fine powder was mixed with commercial transparent flexible resin obtained from Prusa Research a.s., Prague, Czech Republic (tested solid content of glass powder 50 wt%, 52 wt%, 58 wt%, 60 wt%) with Polyethylene glycol (PEG) 5 wt% with respect to the resin weight. The mixture was homogenized with a mechanical mixer at 400 rpm for 10 min.

The 3D printing process was carried out using a masked stereolithography techniques (Prusa SL1S, Prusa Research a.s., Prague, Czech Republic). The geometrical models (STL, Standard Triangulation Language) developed in our previous work [9] were used, with a few changes in the nominal porosity. The gyroid cube structures were printed with 75, and 90 vol% of nominal model porosity with the following printing parameters: layer thickness = 50 μm, and exposure time = 10 s / 3 s. The obtained green body was then detached from its support structures, rinsed in isopropanol/water mixture, post cured by irradiation of the printed structure with a 50 W source at the wavelength of 405 nm using Original Prusa Curing and Washing Machine (CW1S) for about 10 min before carefully moving the printed structure to a furnace for thermal processing. The thermal processing was carried out at different heat treatment regimes, summarized in Table 1.

The densification of glass powder compacts (cylindrical pressed pellets) was examined by hot stage microscopy (HSM) (Leitz, Wetzlar, Germany), operating at a heating rate of 5 °C/min, up to 900 °C. Selected samples were characterized by X-ray powder diffraction (XRD; Bruker D8 Advance, Karlsruhe Germany-CuKα radiation 0.15418 nm), infrared spectroscopy (FTIR 2000, PerkinElmer, Waltham, MA, USA), optical stereomicroscopy (Carl Zeiss Microscopy, New York, USA),

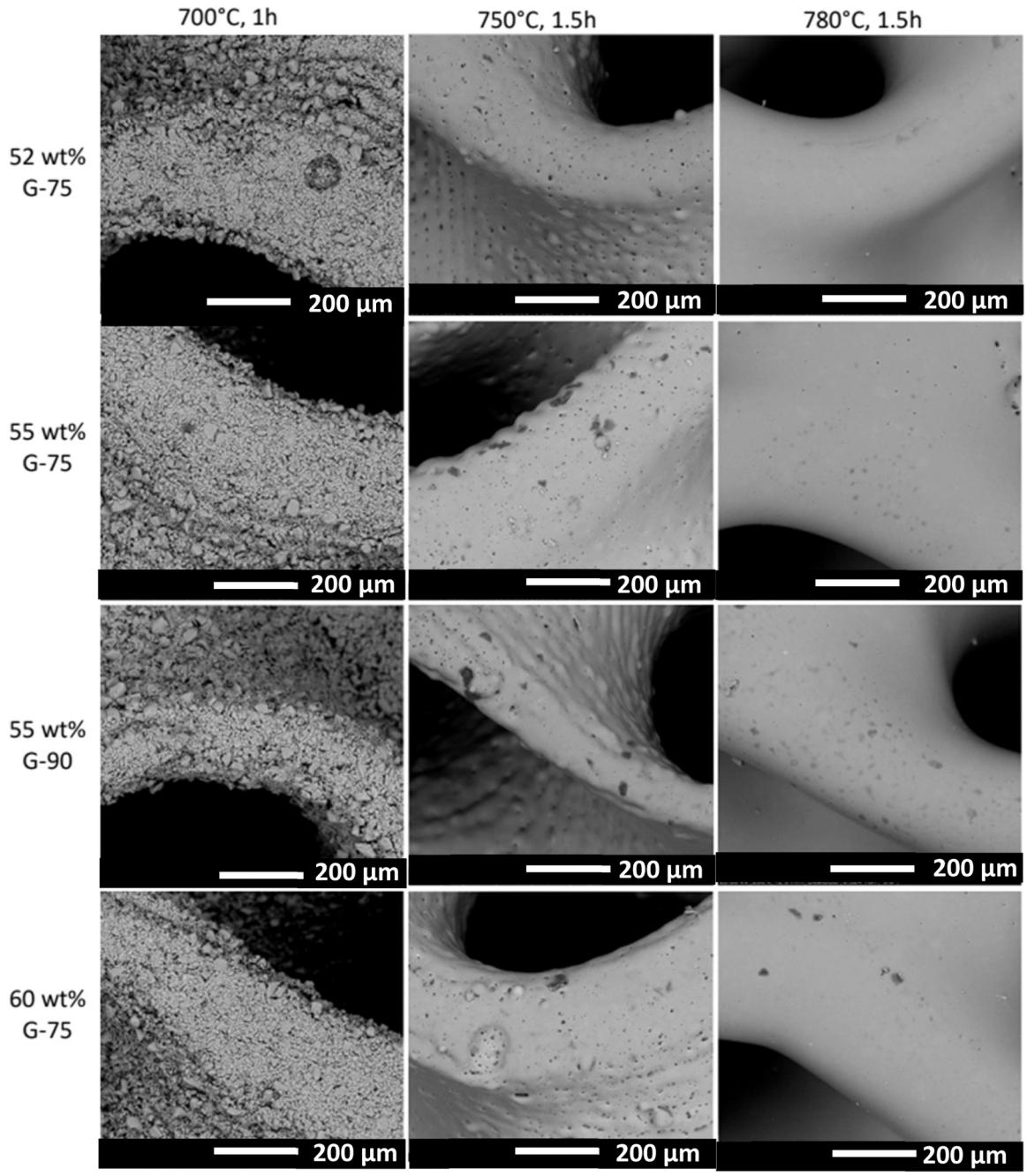

Fig. 4. SEM images of the sintered BSG gyroid scaffolds prepared from slurries with different solid loadings and sintered at different temperatures; the surface roughness decreased with increasing temperature, samples heat-treated at 700 °C and 750 °C retained their shape, although the onset of densification was noticed, while the samples treated at 780 °C displayed a small deformation of the printed structure.

scanning electron microscopy (FEI Quanta 200 ESEM, Eindhoven, The Netherlands) and helium pycnometry (Micromeritics AccuPyc 1330, Norcross, GA). The 3D scaffolds samples were subjected to a compression test, using a universal testing machine (Quasar 25, Galdabini S.p.a., Cardano al Campo, Italy), operating at a crosshead speed of 1 mm/min. Each data point is the average of five independent measurements. The rheological behavior of the suspension was analyzed with a rotation rheometer (Rheometer-viscometer- Haake Mars III). The surface charge on the 3D scaffolds was evaluated by zeta potential measurements on a Litesizer 500 (Anton Paar). The scaffolds were crushed, and a water suspension (pH~ 7) was prepared and sonicated for 20 min before the measurement.

For photocatalytic applications, the selected samples after thermal treatment were dip-coated with TiO_2/binder (Vitroliq P-40) (50:50 wt %) and dried at the room temperature for 24 h. The coated samples were tested for its ability to remove pollutants from water using methylene blue as a reference dye. The 3D BSG scaffolds were placed in beakers containing 100 mL of the dye solution (10 mg/L), under continuous stirring, and left for 60 min in the dark. The suspensions were then irradiated by UV light (Hg lamp, $\lambda = 366$ nm, power = 125 W, Helios Italquartz S.R.L., Milan, Italy). The kinetics and change of concentration of the dye were recorded at pre-defined time intervals using a UV–Vis spectrophotometer (Jasco V570).

The band-gap energy of the scaffolds was determined using the Diffuse reflectance spectra DRS (Jasco V570) and calculated according to the equation for band-gap energy EG (eV)= hc/ λ, where h is Planck's

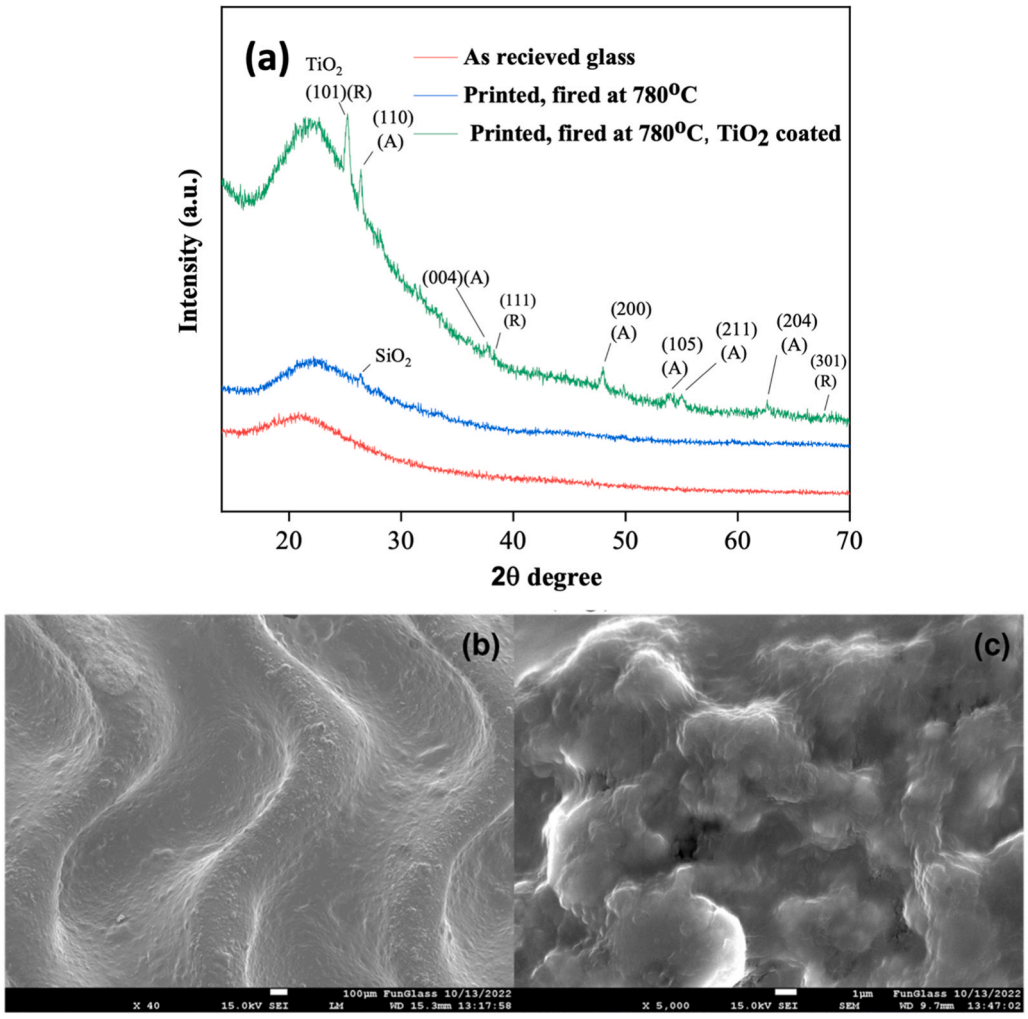

Fig. 5. (a) XRD patterns of as prepared and sintered samples. A – anatase, R - rutile (b,c) SEM micrographs of BSG 750-TiO_2 scaffold at various magnifications, agglomeration of TiO_2 observed on the surface of scaffolds.

constant, c the light velocity (m/s) and λ the wavelength (nm).

3. Results and discussion

3.1. Preliminary sintering studies

Despite extensive studies on glass sintering to produce dense or porous structures, only limited reports are related to AM technology [26]. Achieving highly densified glass structures from glass powders using lithography-based AM is challenging. The key factor is the solid loading and stability of the photocurable slurry to succeed in preparation of suitable green bodies. This is followed by heat treatment involving the removal of the organic moieties and pressureless viscous flow sintering of glass [27]. The glass sintering behavior of the BSG glass powder can be predetermined by hot stage microscopy using glass powder compacts. As shown in Fig. 1, the densification starts around 600 °C and reaches a maximum of around 800 °C. However, at this temperature viscous collapse is observed, which is not favorable for the shaping of high-resolution 3D scaffolds structures. Therefore, it was concluded that an optimized sintering temperature between 700 °C and 800 °C is essential to obtain highly densified translucent glass components.

3.2. Rheological properties of the photocurable slurry

Another crucial step is the formulation of printable slurry consisting of photocurable organic resin (monomers, oligomers and photo-initiators), dispersants and glass powders. Although maximum solid loading may be beneficial for the preparation of highly dense objects, the stability and printability of the slurry must be also considered. Fig. 2 shows the rheological properties of three different slurry formulations with different glass powder solid loadings (52 wt%, 55 wt% and 60 wt %). The suspensions showed typical non-Newtonian, shear thinning behavior. However, the suspension with a high solid loading (60 wt%) of glass powder exhibited shear thickening behavior after 30 min, in contrast with the suspension with a lower solid loading (52 wt%) at the shear rate of 50 s^{-1}. The slurry with 55 wt% solid loading exhibited appreciable time stability, i.e., there were no significant viscosity changes after 30 min setting time.

3.3. MSLA processing

To validate the preliminary studies, the gyroid structures were printed with different slurry formulations and subjected to heat treatment as documented in Table 1. Taking into account the preliminary sintering studies, three different temperatures were selected: 700 °C (TT1), 750 °C (TT2) and 780 °C (TT3). The stereomicroscope images of the BSG gyroid scaffolds (Fig. 3a) demonstrate the effect of different

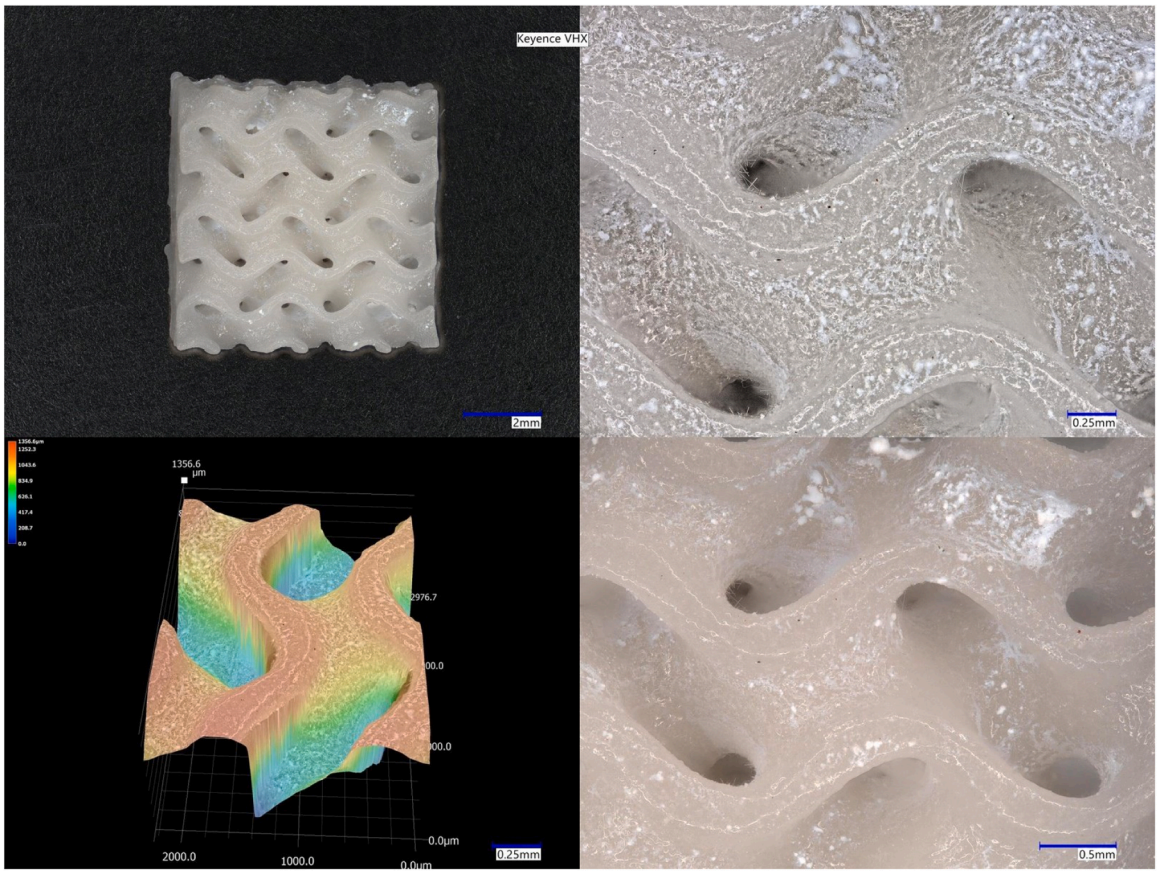

Fig. 6. Optical images of the BSG gyroid scaffolds sintered at 750 (TT2 treatment) and coated with TiO_2 (BSG 750-TiO_2); scaffolds are still translucent and the TiO_2 coating is homogeneous.

Table 2
Physical and mechanical properties of BSG 3D prints; porosity of BSG scaffolds decreased only slightly - from ~74% to ~72% after TiO_2 deposition, no change in the compressive strength was observed.

Samples	Geometrical Density (g/cm^3)	Apparent Density (g/cm^3)	True Density (g/cm^3)	Open Porosity (%)	Closed Porosity (%)	Total Porosity (%)	Compressive strength (MPa)
BSG 3D green	0.42 ± 0.01	1.75 ± 0.01	2.36 ± 0.01	77 ± 2	6 ± 1	83 ± 2	0.92 ± 0.01
BSG 3D 750 °C	0.61 ± 0.01	2.28 ± 0.02	2.40 ± 0.02	72 ± 2	2 ± 0.5	74 ± 2	5.2 ± 2
BSG 3D 750-TiO_2	0.67 ± 0.01	2.31 ± 0.02	2.40 ± 0.02	70 ± 2	2 ± 0.5	72 ± 2	5.2 ± 2

heating temperatures. The samples heat-treated at 700 °C and 750 °C retained their shape, although the onset of densification was noticed, while the samples treated at 780 °C displayed a small deformation of the printed structure. The obtained results are in good agreement with the HSM studies. Also, the surface roughness decreased with increasing temperature (Fig. 4). However, pores were not completely removed, impairing the translucency. Based on the optical and HSM data it was concluded that the gyroid scaffolds treated at 750 °C showed the best results. These were further refined by increasing the porosity to 90%, (Fig. 3c), by reducing the wall thickness, increasing translucency. Therefore, the G-90 3D scaffolds heat treated at 750 °C were selected for further examination. It should be also noted that the sintered samples did not show any discrete diffraction maxima in their XRD patterns, indicating their amorphous (glassy) nature (Fig. 5).

3.4. 3D BSG-TiO_2 scaffolds as photocatalysts

The XRD characterization of the 3D BSG-TiO_2 scaffolds revealed anatase as the predominant crystalline phase and a very low presence of rutile phase (Fig. 5). Diffraction maxima at 2θ = 25.3°, 37.8°, 48.0°, 53.8°, 55°, 62.9° can be indexed to (101), (004), (200), (105), (211), (204) crystal planes of anatase. The reflection at 2θ = 27.4°, 38.2°, 67.8° corresponds to the (110) crystal plane of rutile.

The morphology and homogeneity of the 3D BSG-TiO_2 scaffolds were examined by optical and scanning electron microscopy. Fig. 6 indicates that the scaffolds are still translucent and the TiO_2 coating is homogeneous. Also, no blocking of pores was observed on the optical micrographs, which will ensure efficient water permeation through the scaffolds during photocatalytic tests. This is also confirmed by the results of open porosity measurements shown in Table 2. The porosity of BSG scaffolds decreased only slightly - from ~74% to ~72% after TiO_2 deposition. No change in the compressive strength was observed. Some agglomeration of TiO_2 occurred on the surface of scaffolds, but no cracks were present (Fig. 5b,c).

From the measurement of the surface topography shown in Fig. 6c, three surface profiles were extracted to compute the roughness parameter, which was calculated asRa = 0.154 µm, which is suitable value, compared to the already reported values in context with the effect of semiconductor surface roughness for photocatalytic efficiency [37] Also, the enhanced surface roughness can increase the number of active

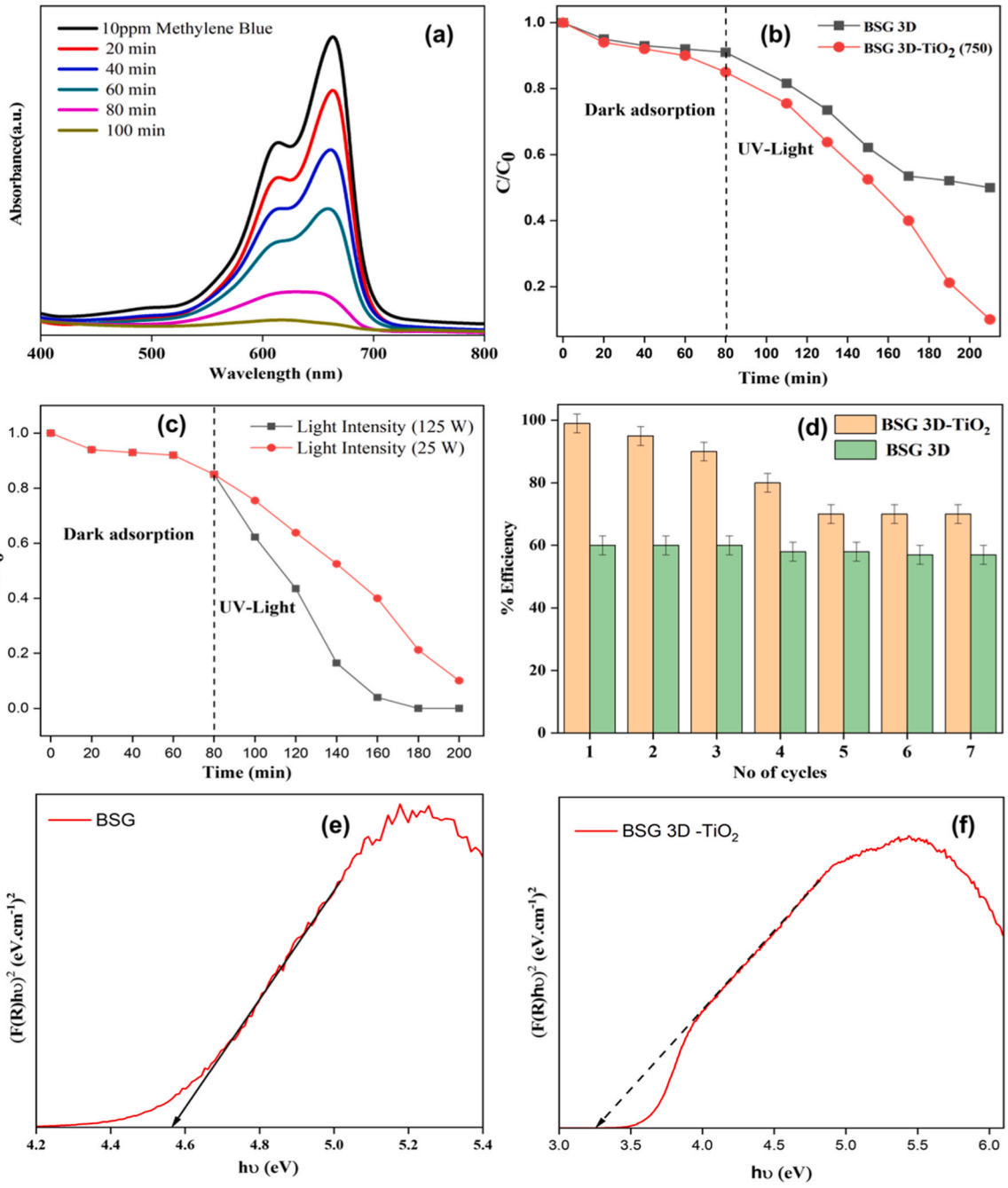

Fig. 7. (a) Concentration changes during photodegradation of methylene blue measured by UV-Visible spectrophotometry; 100% efficiency was achieved within 100 min with 3D BSG-TiO_2. (b) Normalized concentration of MB as a function of irradiation time; in the dark small decrease (20–30%) in the dye concentration observed, because of adsorption of the dye on the catalyst. (c) Normalized concentration of MB as a function of irradiation intensity; the photodegradation rate increased only insignificantly (by ~10–15%) (d) Variation in the efficiency of BSG and BSG 3D-TiO_2 for the degradation of MB with the number of cycles; after seven consecutive cycles the degradation efficiency was still 75% of the original value (e) Band-gap value of BSG 3D (f) Band-gap value of BSG 3D-TiO_2.

sites on the surface of scaffolds, enhancing the photocatalytic performance [38].

A crucial factor for maintaining long-term photocatalytic performance of scaffolds is the stability of TiO_2 coatings on the surface of the scaffolds. The boiling test in water was performed for 15 min: no loss of TiO_2 from the scaffolds was observed, as also confirmed by the weight loss measurement and ICP results.

3.5. Photocatalytic activity of 3D BSG-TiO_2

Methylene blue (MB) was selected as a model dye to evaluate the photocatalytic activity of 3D BSG-TiO_2 under UV-irradiation. The dye is resistant to self-photolysis, so no degradation was observed during photolysis of the dye itself. The test with 3D BSG-TiO_2 in the dark resulted in a small decrease (20–30%) in the dye concentration because of adsorption of the dye on the catalyst. Fig. 7a shows the degradation of MB under UV-light: a 100% efficiency was achieved within 100 min with 3D BSG-TiO_2. A plot of C/C_0 vs irradiation time shows that the concentration of the dye decreased gradually with time (Fig. 7b). Fig. 7 (b) also shows the degradation efficiency of the samples under irradiation for 200 min: it demonstrates that TiO_2 addition enhances the photocatalytic activity and accelerates the process of the photodegradation

Table 3
Comparison table of different photocatalysts with the degradation efficiency.

Photocatalyst	Light source	Degradation time	Reference
Fe_3O_4/TiO_2 Nano-Catalyst	UV light (1000 W)	100% in 60 min	[28]
ZSM-5/TiO_2/Ni	UV light (16 W)	100% in 120 min	[29]
Glass substrate/TiO_2	UV light (15 W)	97.6 in 180 min	[30]
N-doped TiO_2/SiO_2	LED light (16 W)	70% in 12 h	[31]
Co–TiO_2	White Compact Fluorescent lamp (23 W)	100% in 360 min	[32]
Glass Fiber/TiO_2	UV light	70% in 100 min	[33]
3D BSG-TiO_2	UV light (366 nm, 25 W)	100% in 100 min	Present work

reaction. Compared with uncoated BSG 3D scaffolds, the degradation efficiency of BSG 3D scaffolds coated with TiO_2 is improved by 40%. Moreover, the efficiency of the present photocatalysts (3D BSG-TiO_2) is comparable to existing photocatalysts as depicted in Table 3.

Another important factor to notice was the trend in the concentration of dye with respect to irradiation intensity. By increasing the irradiation intensity from 25 Wcm^2 to 125 W cm^2, the photodegradation rate increased only insignificantly (by ~10–15%): this indicates that the total light energy accumulated by TiO_2 which leads to faster oxidative photodegradation reached its maximum already at a lower irradiation intensity (Fig. 7c). In addition, the persistence of photocatalytic efficiency of the scaffolds was assessed. After seven consecutive cycles the degradation efficiency was still 75% of the original value, which confirms the stability of the system (Fig. 7f). The photodegradation efficiency was calculated according to the equation:

$$\eta(\%) = 100 * \frac{(C0 - Ct)}{C0}$$

where η is the photodegradation efficiency, C_0 is the initial concentration of MB before the reaction, and Ct is the equilibrium concentration of MB at the irradiation time t. Moreover, Fig. 7g indicates that approximately 10 wt% of TiO_2 is still present on the surface of 3D BSG-TiO_2 scaffolds after 7 cycles, which is an important factor in maintaining the photocatalytic efficiency.

3.6. Proposed mechanism

The MB absorbance band appears at 664 nm (Fig. 7a) It was shifted to 620 nm after 60 min and to 610 nm after 100 min of the UV-exposure. The reason is demethylation of MB which results in the blue shift of the absorbance band [34]. Previous studies also concluded that the absence of the absorbance peak in the visible spectrum range of 600–664 nm indicates a complete decomposition of MB dye [35,36]. Along with photodegradation, adsorption is also playing part because of the high porosity of BSG 3D-TiO_2. ζ-potential measurements determined that the surface of BSG 3D-TiO_2 scaffold was negatively charged (−25 mV) so that the dye molecules could be adsorbed on the surface of the scaffold due to electrostatic interaction between the cationic MB dye and negative charges on the BSG 3D -TiO_2 scaffold. This leads to a noticeable decrease in the concentration of the dye in the solution, which is followed by their complete photodegradation. The mechanism of complete decomposition of MB is outlined in Fig. 8. In BSG 3D -TiO_2, two main oxide semiconductors (SiO_2 and TiO_2) are combined, but more effective role is believed to be played by TiO_2 as it is present on the surface of the scaffold. SiO_2 is typically used as a catalyst support, and achieving a highly porous 3D structure from BSG glass represents an advantage. As structures with high porosity have a large internal surface area per weight, it is this property that provides high accessibility and diffusivity that allow molecules penetrate through pores, resulting in higher degradation of pollutants on the catalyst's surface [39]. When the BSG 3D-TiO_2 is exposed to a photon of suitable energy the electrons in the valance band of TiO_2 are excited to the conduction band creating an electron–hole pair. Most excited electrons are transferred from the TiO_2 conduction band into BSG (SiO_2) because the outer surface of the scaffolds is covered by TiO_2. TiO_2 has a smaller band gap (Fig. 7d, e). An equivalent number of holes generated in the VB of the TiO_2 layer will directly react with the MB dye molecule [40,41]. This minimizes the recombination rate and facilitates the migration of electrons to the surface of the scaffold where the charges participate in the photodecomposition of MB dye. This hypothesis is supported by the bandgap energy values shown in Fig. 7d. The proposed mechanism takes place in three steps; Initially, the oxidation step where the holes (h^+) react with H_2O or with hydroxyl groups (OH^-) on the surface of the scaffold to produce the hydroxyl radicals (OH•) and the H^+ ions. Secondly, the reduction step where O_2 adsorbed on the surface of the scaffold can be reduced by the electrons to generate superoxide anions ($O^{2\bullet-}$), Then formed $O^{2\bullet-}$ anions react with hydrion (H^+) discharged in the first step

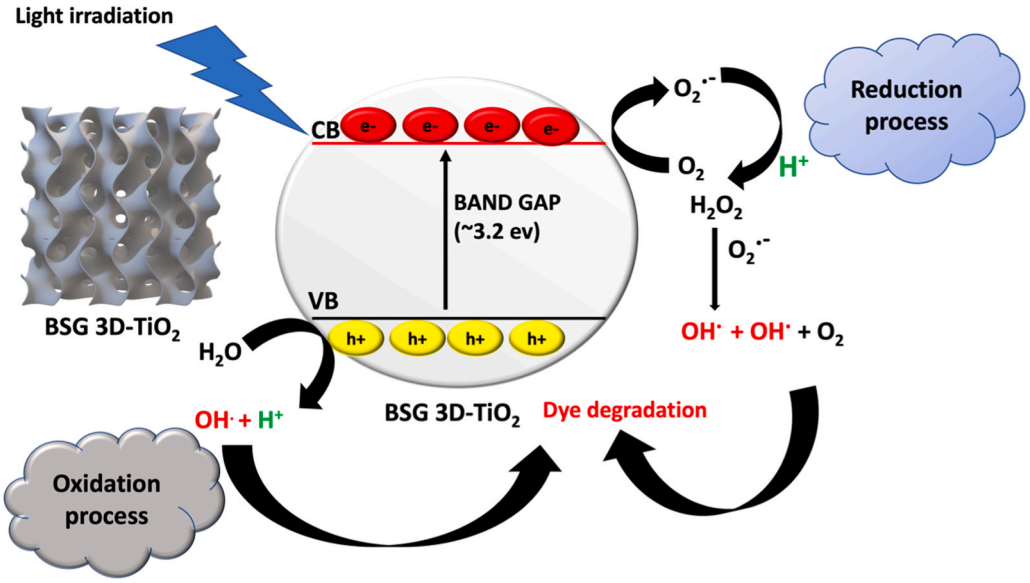

Fig. 8. Proposed mechanism of photodegradation of MB by BSG 3D-TiO_2.

to produce more of hydroxyl radicals (OH•). Lastly, the generated strongly oxidizing hydroxyl radicals (OH•) decompose the MB dye.

4. Conclusion

The complete route for shaping of waste BSG glass with polymeric resin for the manufacturing of 3D gyroid scaffold-like membranes by stereolithography was established. The parameters like solid content and stability of polymeric inks, and removal of the organic moieties after heat treatment were reviewed and optimized. The optimized sintering temperature between 700 °C to 800 °C is essential to obtain highly densified translucent glass components. The gyroid structures were printed with different slurry formulations. The best results were obtained at 55 wt% solid BSG loading and the sintering temperature of 750 °C. The scaffolds were further refined by increasing its overall porosity to 90% through thinning of strut walls, leading to translucent bodies. The 3D scaffolds with the mechanical strength of 5.2 MPa and coated by TiO_2 were employed for heterogenous photocatalytic degradation of methylene blue used as a reference, resulting in 100% photocatalytic degradation of the dye in 100 min. The study resolved the number of barriers concerning the 3D printing of complex structures from waste glass, outlining potential avenues for their utilization in water treatment applications.

Environmental importance

In a sustainable society, the recovery of waste materials and energy by following the circular economy is a challenging task. This concept targets to protect end-of-life materials at their highest effective utility while minimizing negative impacts. In accordance with this idea, we developed a methodological approach to upcycle BSG waste using additive manufacturing SL technique.

CRediT authorship contribution statement

Akansha Mehta: Methodology, analysis, conceptualization, Data curation, writing. **Paulina Ozog: F**ormal analysis, Investigation, Data curation. **Arish Dasan:** Software, Methodology. **Jozef Kraxner:** Resources, Supervision, Project administration. **Hamada Elsayed:** Conceptualization. **Luca Grigolato: S**oftware. **Dusan Galusek:** Writing – review & editing, Funding acquisition. **Enrico Bernardo**: Supervision, Resources, Writing – original draft preparation. All authors have read and agreed to the published version of the manuscript.

Declaration of Competing Interest

The authors declare that they have no known competing financial interests or personal relationships that could have appeared to influence the work reported in this paper.

Acknowledgment

This paper is a part of the dissemination activities of project FunGlass (Centre for Functional and Surface Functionalized Glass). This project has received funding from the European Unionś Horizon 2020 research and innovation programme under grant agreement No 739566. The authors also acknowledge Gianpaolo Savio for the modelling of gyroid cube structures.

References

[1] J.M. Lessard, G. Habert, A. Tagnit-Hamou, B. Amor, Tracking the environmental consequences of circular economy over space and time: the case of close-and open-loop recovery of postconsumer glass, Environ. Sci. Technol. (17) (2021) 11521–11532, https://doi.org/10.1021/acs.est.1c03074.

[2] C. Shi, K. Zheng, 2007. A review on the use of waste glasses in the production of cement and concrete, Resour. Conserv. Recycl., 2(2007), pp. 234–247, https://doi.org/10.1016/j.resconrec.2007.01.013.

[3] A. Saccani, S. Manzi, I. Lancellotti, L. Barbieri, Manufacturing and durability of alkali activated mortars containing different types of glass waste as aggregates valorisation, Constr. Build. Mater. 237 (2020), 117733, https://doi.org/10.1016/j.conbuildmat.2019.117733.

[4] D. Robert, E. Baez, S. Setunge, A new technology of transforming recycled glass waste to construction components, Constr. Build. Mater. 313 (2021), 125539. ⟨https://doi.org/10.1016/j.conbuildmat.2021.125539⟩.

[5] D. Ramteke, M. Hujova, J. Kraxner, D. Galusek, A.R. Romero, R. Falcone, E. Bernardo, Up-cycling of unrecyclable glasses in glass-based foams by weak alkali-activation, gel casting and low-temperature sintering, J. Clean. Prod. 278 (2021), 123985. ⟨https://doi.org/10.1016/j.jclepro.2020.123985⟩.

[6] W. Dong, W. Li, Z. Tao, A comprehensive review on performance of cementitious and geopolymeric concretes with recycled waste glass as powder, sand or cullet, Resour. Conserv. Recycl. 172 (2021), 105664, https://doi.org/10.1016/j.resconrec.2021.105664.

[7] A. Mehta, K. Karbouche, J. Kraxner, H. Elsayed, D. Galusek, E. Bernardo, Upcycling of pharmaceutical glass into highly porous ceramics: from foams to membranes, Materials (11) (2022) 3784, https://doi.org/10.3390/ma15113784.

[8] J. Savolainen, M. Collan, How additive manufacturing technology changes business models–review of literature, Addit. Manuf. 32 (2020), 101070, https://doi.org/10.1016/j.addma.2020.101070.

[9] A. Dasan, P. Ożóg, J. Kraxner, H. Elsayed, E. Colusso, L. Grigolato, E. Bernardo, Up-cycling of LCD glass by additive manufacturing of porous translucent glass scaffolds, Materials 14 (2021) 5083, https://doi.org/10.3390/ma14175083.

[10] T. Peng, K. Kellens, R. Tang, C. Chen, G. Chen, Sustainability of additive manufacturing: an overview on its energy demand and environmental impact, Addit. Manuf. 21 (2018) 694–704, https://doi.org/10.1016/j.addma.2018.04.022.

[11] H. Tetik, Y. Wang, X. Sun, D. Cao, N. Shah, H. Zhu, D. Lin, Additive manufacturing of 3D aerogels and porous scaffolds: a review, Adv. Funct. Mater. 31 (2021), 2103410, https://doi.org/10.1002/adfm.202103410.

[12] S.H. Siddique, P.J. Hazell, H. Wang, J.P. Escobedo, A.A. Ameri, Lessons from nature: 3D scaffolds bio-inspired porous structures for impact energy absorption–A review, Addit. Manuf. 58 (2022) (2022), 103051, https://doi.org/10.1016/j.addma.2022.103051.

[13] T.D. Ngo, A. Kashani, G. Imbalzano, K.T. Nguyen, D. Hui, Additive manufacturing (3D printing): a review of materials, methods, Appl. Chall. Compos. B. Eng. 143 (2018) 172–196, https://doi.org/10.3390/app12073591.

[14] M.L. Griffith, J.W. Halloran, Freeform fabrication of ceramics via stereolithography, J. Am. Ceram. 79 (1996) 2601–2608, https://doi.org/10.1111/j.1151-2916.1996.tb09022.x.

[15] E.J. Parteli, J. Schmidt, C. Blümel, K.E. Wirth, W. Peukert, T. Pöschel, Attractive particle interaction forces and packing density of fine glass powders, Sci. Rep. 4 (2014), 6227, https://doi.org/10.1038/srep06227.

[16] H. Elsayed, P. Colombo, M.C. Crovace, E.D. Zanotto, E. Bernardo, Suitability of Biosilicate glass-ceramic powder for additive manufacturing of highly porous scaffolds, Ceram. Int. 47 (2021) 8200–8207, https://doi.org/10.1016/j.ceramint.2020.11.179.

[17] H. Dommati, S.S. Ray, J.C. Wang, S.S. Chen, A comprehensive review of recent developments in 3D printing technique for ceramic membrane fabrication for water purification, RSC Adv. 9 (2019) 16869–16883, https://doi.org/10.1039/C9RA00872A.

[18] R.S. Dongre, K.K. Sadasivuni, K. Deshmukh, A. Mehta, S. Basu, J.S. Meshram, A. Karim, Natural polymer based composite membranes for water purification: a review, Polym. Plast. Tech. Mat. 58 (2019) 1295–1310, https://doi.org/10.1080/25740881.2018.1563116.

[19] O.M. Rodriguez-Narvaez, J.M. Peralta-Hernandez, A. Goonetilleke, E.R. Bandala, Treatment technologies for emerging contaminants in water: a review, J. Chem. Eng. 323 (2017) 361–380, https://doi.org/10.1016/j.scitotenv.2020.141990.

[20] L. Pereira, M. Alves, Dyes—environmental impact and remediation, Environ. Prot. Strateg. Sustain. Dev. (2012) 111–162.

[21] A. Mishra, A. Mehta, S. Basu, Clay supported TiO_2 nanoparticles for photocatalytic degradation of environmental pollutants: a review, J. Environ. Chem. Eng. 6 (2018) 6088–6107, https://doi.org/10.1016/j.jece.2018.09.029.

[22] K. Nakata, A. Fujishima, TiO_2 photocatalysis: design and applications, J. Photochem. Photobiol. C. Rev. 13 (2012) 169–189, https://doi.org/10.1016/j.jphotochemrev.2012.06.001.

[23] S.S. Marzouk, V. Naddeo, F. Banat, S.W. Hasan, Preparation of TiO_2/SiO_2 ceramic membranes via dip coating for the treatment of produced water, Chemosphere 273 (2021), 129684, https://doi.org/10.1016/j.chemosphere.2021.129684.

[24] Q. Zhang, H. Wang, X. Fan, F. Lv, S. Chen, X. Quan, Fabrication of TiO_2 nanofiber membranes by a simple dip-coating technique for water treatment, Surf. Coat. Technol. 298 (2016) 45–52, https://doi.org/10.1016/j.surfcoat.2016.04.054.

[25] Y. Lakhdar, C. Tuck, J. Binner, A. Terry, R. Goodridge, Additive manufacturing of advanced ceramic materials, Prog. Mater. Sci. 116 (2021), 100736, https://doi.org/10.1016/j.pmatsci.2020.100736.

[26] A.K. Hofer, A. Kocjan, R. Bermejo, High-strength lithography-based additive manufacturing of ceramic components with rapid sintering, Addit. Manuf. 59 (2022), 103141, https://doi.org/10.1016/j.addma.2022.103141.

[27] S. Moosavi, R.Y. Li, C.W. Lai, Y. Yusof, S. Gan, et al., Methylene blue dye photocatalytic degradation over synthesised Fe_3O_4/AC/TiO_2 nano-catalyst: degradation and reusability studies, Nanomater 10 (2020) 2360, https://doi.org/10.3390/nano10122360.

[28] K. Badvi, V. Javanbakht, Enhanced photocatalytic degradation of dye contaminants with TiO2 immobilized on ZSM-5 zeolite modified with nickel nanoparticles, J. Clean. Prod. 280 (2021), 124518, https://doi.org/10.1016/j.jclepro.2020.124518.

[29] A. Bouarioua, M. Zerdaoui , 2017. Photocatalytic activities of TiO2 layers immobilized on glass substrates by dip-coating technique toward the decolorization of methyl orange as a model organic pollutant. J. Environ. Chem. Eng., 5(2017), pp.1565–74, https://doi.org/10.1016/j.jece.2017.02.025.

[30] S. Samangsri, T. Areerob, S. Chiarakorn, Development of visible light-responsive N-doped TiO2/SiO2 core–shell nanoparticles for photocatalytic degradation of methylene blue dye, 1649-64, Res. Chem. Intermed. 49 (2023), https://doi.org/10.1007/s11164-022-04925-0, 1649-64.

[31] A. El. Mragui, O. Zegaoui, J.C. da, Silva, Elucidation of the photocatalytic degradation mechanism of an azo dye under visible light in the presence of cobalt doped TiO_2 nanomaterials, Chemosphere 266 (2021), 128931, https://doi.org/10.1016/j.chemosphere.2020.128931.

[32] S. Fukugaichi , 2019. Fixation of titanium dioxide nanoparticles on glass fiber cloths for photocatalytic degradation of organic dyes. ACS omega. 2019 4(2019), pp. 15175–80, https://doi.org/10.1021/acsomega.9b02067.

[33] U. Mahanta, M. Khandelwal, A.S. Deshpande, TiO_2@SiO_2 nanoparticles for methylene blue removal and photocatalytic degradation under natural sunlight and low-power UV light, Appl. Surf. Sci. 576 (2022), 151745, https://doi.org/10.1016/j.apsusc.2021.151745.

[34] T. Zhang, T. Oyama, A. Aoshima, H. Hidaka, J. Zhao, N. Serpone, Photooxidative N-demethylation of methylene blue in aqueous TiO_2 dispersions under UV irradiation, J. Photochem. Photobiol., A 140 (2001) 163–172, https://doi.org/10.1016/S1010-6030(01)00398-7.

[35] H. Jafari, S. Afshar, Improved photodegradation of organic contaminants using nano-TiO_2 and TiO_2–SiO_2 deposited on Portland cement concrete blocks, J. Photochem. Photobiol. 92 (2016) 87–101, https://doi.org/10.1111/php.12554.

[36] I. Kim, S. Kim, A. Andreu, J.H. Kim, Y.J. Yoon, Influence of dispersant concentration toward enhancing printing precision and surface quality of vat photopolymerization 3D printed ceramics, Addit. Manuf. 52 (2022), 102659, https://doi.org/10.1016/j.addma.2022.102659.

[37] L. Xu, G. Zheng, F. Xian, J. Su, The morphological evolution of ZnO thin films by Sn ions doping and its influence on the surface energy and photocatalytic activity, Mater. Chem. Phys. 229 (2019) 215–225, https://doi.org/10.1016/j.matchemphys.2019.03.011.

[38] C.G. Joseph, Y.H. Taufiq-Yap, B. Musta, M.S. Sarjadi, L. Elilarasi, Application of plasmonic metal nanoparticles in TiO_2-SiO_2 composite as an efficient solar-activated photocatalyst: a review paper, Front. Chem. 8 (2021), 568063, https://doi.org/10.3389/fchem.2020.568063.

[39] Z.Y. Yang, G.Y. Shen, Y.P. He, X.X. Liu, S.J. Yang, Preparation of TiO_2/SiO_2 composite oxide and its photocatalytic degradation of rhodamine B, J. Porous Mater. 23 (2016) 589–599, https://doi.org/10.1007/s10934-015-0114-7.

[40] W. Chen, C. Takai, H.R.Khosroshahi, M. Fuji, T. Shirai, 2016. SiO_2/TiO_2 double-shell hollow particles: fabrication and UV–Vis spectrum characterization. Adv Powder Technol., 27(2016), pp. 812–818, https://doi.org/10.1016/j.apt.2015.10.016.